https://doi.org/10.5194/egusphere-2026-3947
Preprint. Discussion started: 14 July 2026

Purely light-scattering aerosols could induce positive shortwave radiative forcing over high-albedo surfaces

Longrui Zhang[1], Taveen S. Kapoor[1], Prabhav Upadhyay[1], and Rajan K. Chakrabarty[1]

[1]Department of Energy, Environmental and Chemical Engineering, Washington University in St. Louis, St. Louis, MO 63130, USA

Correspondence: Taveen S. Kapoor (taveensk@gmail.com), Rajan K. Chakrabarty (chakrabarty@wustl.edu)

Abstract. Anthropogenic particles enter the stratosphere both by design and by accident: stratospheric aerosol injection (SAI) proposes deliberate particle injection to partially counteract global warming by increasing planetary albedo, while spacecraft reentry ablation already deposits alumina in stratospheric aerosol at rates growing with launch activity. Scattering particle layers in the stratosphere are conventionally expected to cool the surface; however, their radiative behavior over high-albedo surfaces remains under-examined. This study investigates the counter-intuitive positive shortwave radiative forcing induced by purely scattering aerosols over bright surfaces such as snow and ice. By conducting radiative transfer simulations of an SAI-relevant aerosol layer with libRadtran, we compare the rigorous discrete-ordinate method (DISORT) against the standard two-stream approximation commonly utilized in climate models. We identify significant positive forcing at low solar zenith angles over high-albedo regions, a phenomenon systematically underestimated by the two-stream approximation. To elucidate the mechanism, we derive a first-principles "single-layer adding model" that attributes this positive forcing to the optical path length asymmetry between collimated downwelling solar radiation and diffuse upwelling radiation. We introduce the reflectance asymmetry parameter (Φ) to quantify this asymmetry: diffuse upwelling light encounters a longer optical path through the layer and is preferentially backscattered to the surface. Furthermore, we show that standard daily-averaged forcing metrics obscure these strong diurnal forcing peaks, potentially masking critical impacts on snowmelt. These findings suggest that current assessments may underestimate the localized climatic risks of SAI and extend to any optically thin scattering layer over bright surfaces – including the growing burden of reentry-derived alumina.

1 Introduction

Stratospheric aerosol injection (SAI) is a proposed form of solar radiation modification (SRM) that aims to contribute to counteracting global warming by injecting reflective particles into the stratosphere (Crutzen, 2006). The concept draws inspiration from major volcanic eruptions, which inject large quantities of sulfur dioxide (SO_2), which oxidize to sulfate aerosols in the stratosphere and have been observed to produce measurable global cooling (Robock, 2000). Motivated by this natural analogue, studies model sulfate aerosol injections into the stratosphere to understand their radiative and climate impacts. Alternative materials such as solid particle oxides and diamond are also under active investigation owing to their

https://doi.org/10.5194/egusphere-2026-3947
Preprint. Discussion started: 14 July 2026

potentially favorable optical and chemical properties (Pope et al., 2012; Dykema et al., 2016). Alumina, a leading solid-particle candidate, is moreover no longer hypothetical in the stratosphere: in situ measurements show that spacecraft reentry ablation already deposits aluminum-bearing particles in stratospheric aerosol (Murphy et al., 2023), a source projected to grow with rising launch and reentry rates. Regardless of the choice of material – or whether the layer is deliberate or inadvertent – the radiative forcing produced by a stratospheric particle layer depends not only on the particle's intrinsic optical properties but also on environmental conditions and the numerical methods used to model radiative transfer, factors that remain insufficiently characterized.

Quantifying the climatic impact of SAI requires solving the radiative transfer equation (RTE) to compute the aerosol direct radiative forcing (ADRF), defined as the change in net radiative flux at the top of the atmosphere due to the presence of aerosols. Intrinsic aerosol optical parameters entering the RTE include the extinction coefficient, the single-scattering albedo (SSA), and the scattering phase function, all of which are determined by particle size distribution and complex refractive index. Because SAI remains a conceptual intervention, its climatic effects are primarily explored through general circulation models (GCMs). To remain computationally tractable, most GCMs solve the RTE using a two-stream approximation, which represents the radiation field with one upward and one downward beam. The widely used Rapid Radiative Transfer Model for GCMs (RRTMG) is based on this two-stream approach and is employed in major climate models such as CESM (Community Earth System Model), E3SM (Energy Exascale Earth System Model) and SOCOL-AERv2 (Iacono et al., 2008; Danabasoglu et al., 2020; Vattioni et al., 2024). However, more rigorous methods, such as the discrete-ordinate method (DISORT), resolve the angular distribution of intensity with far greater fidelity (Stamnes et al., 1988). Intercomparison studies have shown that differences in the treatment of multiple scattering among radiative transfer schemes contribute to 10 – 20% discrepancies in modeled ADRF (Randles et al., 2013).

Beyond the inputs of aerosol optical properties and choice of radiative transfer solver, two environmental inputs to the RTE – solar zenith angle (SZA) and surface albedo – exert a strong influence on the magnitude and even the sign of ADRF, yet the mechanisms governing this sensitivity are not well established. Derimian et al. (2016) demonstrated that systematic biases between the two-stream approximation and Discrete Ordinates Radiative Transfer solver (DISORT) depend on both SZA and surface albedo. Atwater (1970) showed analytically that aerosols over high-albedo surfaces can produce positive ADRF, though the analysis employed a simplified single-scattering framework. Using a numerical global climate model, Brovkin et al. (2009) found that simulated stratospheric sulfate injection produced warming of 0.5–1 °C over the Tibetan Plateau and North Africa, regions of high surface albedo where the addition of an aerosol layer lowers rather than raises planetary albedo. They attributed the regional warming to multiple scattering between the layer and the bright surface enhancing solar absorption. More recently, analyses from Clouds and the Earth's Radiant Energy System (CERES) satellite similarly identify a critical surface albedo above which the observed aerosol direct radiative effect becomes positive, attributed primarily to surface-amplified absorption by weakly absorbing aerosols (Chen et al., 2024). Both studies use aerosols with SSA very close to but

https://doi.org/10.5194/egusphere-2026-3947
Preprint. Discussion started: 14 July 2026

not exactly to 1, leaving open whether the sign reversal can occur in the strict pure-scattering limit. Further, if non-absorbing (i.e., purely-scattering) particles do introduce a positive forcing, what is the underlying mechanism for the same. This question is not purely hypothetical: in situ measurements show that spacecraft reentry ablation already deposits alumina and other metal particles in stratospheric aerosol (Murphy et al., 2023), a source projected to grow with rising launch and reentry rates, so the radiative behavior of purely scattering particles over bright surfaces is relevant even in the absence of deliberate injection.

In this study, we investigate this positive-forcing phenomenon using offline radiative transfer simulations with the libRadtran package, comparing DISORT against the two-stream method across a range of SZA and surface albedo values. Our simulations reveal that even for pure scatterers, ADRF becomes positive over high-albedo surfaces at low SZA – a signal that is significantly more pronounced in DISORT than in the two-stream approximation. To explain the underlying physics, we derive a single-layer adding model that attributes the positive forcing to an optical path length asymmetry between the collimated downwelling solar beam and the diffuse upwelling radiation reflected by the surface, which we term the "reflectance asymmetry" mechanism. The robustness of this mechanism is evaluated by testing the dependence of Φ on solar geometry and independence to the underlying surface albedo, which numerical radiative transfer simulations confirm. These findings highlight a previously uncharacterized risk of SAI deployment and suggest that current GCM-based assessments, relying on two-stream solvers and daily-averaged forcing, may systematically underestimate localized warming over bright surfaces.

2 Method for numerical modeling

2.1 Radiative transfer model setup

To investigate the sensitivity of aerosol direct radiative forcing (ADRF) to surface albedo, SZA, and the treatment of multiple scattering, we constructed a plane-parallel, single-layer radiative transfer model representing a homogeneous aerosol slab in the stratosphere above a Lambertian surface. The model computes the shortwave radiative transfer over the spectral range of 250 nm to 3000 nm, consistent with the usually used shortwave band of solar radiation (Oke, 2018).
The injected aerosol layer was placed between 18 km and 23 km altitude, corresponding to the lower stratosphere where proposed SAI deployment would occur (Dykema et al., 2016; Weisenstein et al., 2015). The aerosol was modeled as purely scattering alumina (imaginary refractive index set to zero) to isolate the geometric scattering effects from absorption. A lognormal particle size distribution was assumed with a mean diameter of 430 nm, a geometric standard deviation of 1.5, and a number concentration of 11 #/cm^3; similar to the parameters used by Dykema et al. (2016) to cause a 1 W m^{-2} of radiative forcing by alumina particles. Refractive indices of alumina were taken from Tropf and Thomas (1997). No background atmospheric molecular scattering or absorption was included in this configuration, so the results should be interpreted in terms of trends rather than absolute values; this point is revisited in the discussion of Fig. 1.

https://doi.org/10.5194/egusphere-2026-3947
Preprint. Discussion started: 14 July 2026

The radiative transfer equation (RTE) was solved using two methods to evaluate the impact of multiple scattering treatment on ADRF: (1) the Roberts Delta-Eddington Two-Stream solver (RODENTS), representative of the two-stream approximations employed in most general circulation models (Zdunkowski et al., 2007), and (2) the 16-stream DISORT solver, which resolves the angular distribution of intensity with higher fidelity (Stamnes et al., 1988). Both solvers were implemented via the libRadtran software package, version 2.0.5 (Emde et al., 2016). Simulations were performed across surface albedo values from 0 to 1 and SZA values from 0° to 90° to simulate plausible ranges of influence of diurnal and latitudinal changes to radiative forcing.

The solution to the RTE provides instantaneous upward spectral irradiance ($F_\lambda^\uparrow$) at the top of the atmosphere (TOA). The broadband upward irradiance ($F\uparrow$) is obtained by spectral integration over the 250 nm to 3000 nm wavelengths, representing the shortwave spectral range. The broadband downward irradiance at the TOA, representing the incident solar radiation, is denoted S(μ), where $\mu = \cos\theta$ and θ is the SZA. The ADRF is then defined as the change in net upward flux at the TOA due to the presence of the aerosol layer:

$$ADRF = (S - F^\uparrow_{after\ injection}) - (S - F^\uparrow_{no\ injection}) = F^\uparrow_{no\ injection} - F^\uparrow_{after\ injection}$$

2.2 Aerosol optical properties

The aerosol optical properties required as input to the RTE–extinction coefficient, SSA, and scattering phase function–were computed using Mie theory as implemented in the PyMieScatt Python library (Sumlin et al., 2018). Wavelength-dependent refractive indices of alumina from Tropf and Thomas (1997) were used as input, and the optical properties were calculated over the spectral range of 250 nm to 3000 nm.

The scattering phase function was expanded in Legendre polynomials to provide the angular scattering representation required by DISORT. The expansion was truncated at 17 moments (nmom = 17), and the Legendre coefficients were computed following the pmom function from libRadtran (Emde et al., 2016). Details of the Legendre polynomial fitting procedure, including the normalization condition, recurrence relation, and numerical quadrature method, are provided in Sect. S1 of the Supplement.

2.3 Daily-averaged ADRF

To assess whether the positive ADRF identified at specific SZA values persists when averaged over a full diurnal cycle, we computed the daily-mean ADRF for three latitude bands (0–30° N, 30–60° N, and 60–90° N) for June 21st (northern hemisphere summer solstice, 2025). For each band, an area-weighted effective latitude ϕ_{eff} was calculated using cosine weighting to account for the spherical geometry of the Earth, and the diurnal variation of SZA was computed from standard solar geometry using the Fourier-series approximation for solar declination (Duffie and Beckman, 2013). The instantaneous ADRF was then averaged over daylight hours. The full mathematical formulation of the averaging procedure, including the effective latitude calculation and SZA time dependence, is provided in Sect. S2 of the Supplement.

https://doi.org/10.5194/egusphere-2026-3947
Preprint. Discussion started: 14 July 2026

3 Results and discussion

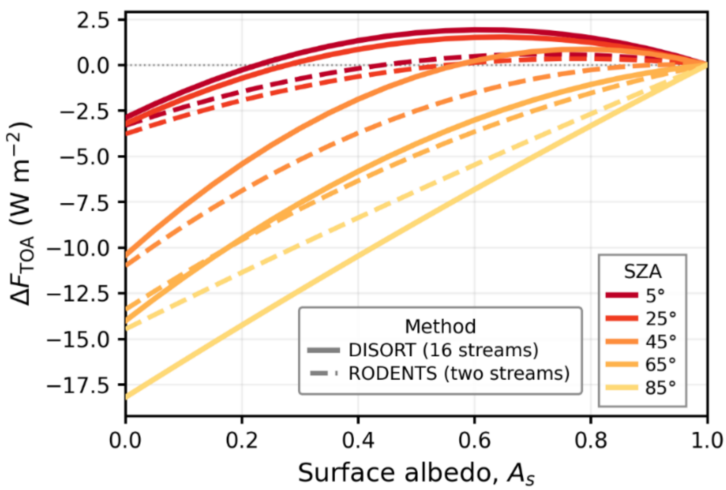

Figure 1 Illustration of the sensitivity of ADRF to surface albedo, SZA, and the multiple scattering treatment (DISORT vs. RODENTS) following the injection of pure scattering alumina aerosols. Injected alumina follows the lognormal distribution with mean diameter 430nm, geometric standard deviation 1.5 and number concentration 11 $\#/cm^3$. The injection height is between 18km to 23km (stratosphere).

Figure 1 shows the sensitivity of shortwave ADRF to surface albedo (A_s) and SZA for purely scattering alumina aerosols. As described in Sect. 2.1, this configuration excludes background atmospheric absorption, so the numerical values should be interpreted as illustrative of trends rather than quantitative predictions of real-world forcing. At high SZA (e.g., θ = 85°), ADRF is negative across all surface albedo values in both solvers, consistent with the familiar expectation that a scattering aerosol layer increases planetary albedo and produces negative shortwave radiative forcing. When SZA > 85°, ADRF expectedly approaches zero (Fig. S2) as it should be, since the incident solar flux on a horizontal plane scales with cos (SZA) and vanishes at grazing incidence, leaving no shortwave energy for the layer to redistribute.

However, at lower SZA (e.g., $\theta < 45°$) the sign of ADRF becomes more complicated: ADRF initially grows (less negative forcing) with increasing A_s, and crosses zero to become positive. It reaches a maximum (e.g., ADRF = +2 W m^{-2} at $\theta = 5°$, A_s = 0.6, using DISORT solver), and then decreases to zero at A_s = 1. Positive ADRF indicates a net reduction in the flux reflected to space despite the aerosol being purely scattering. Similar sign reversals have been previously documented in global simulations using stratospheric sulfate (Brovkin et al., 2009, 0.5–1 °C warming over the Tibetan Plateau and North Africa)

https://doi.org/10.5194/egusphere-2026-3947
Preprint. Discussion started: 14 July 2026

and in satellite analyses (Chen et al., 2024). These earlier studies attribute the positive forcing to multiple-scattering-enhanced absorption by weakly absorbing aerosols. The present results demonstrate that an analogous sign reversal arises despite an absence of absorption. We describe this phenomenon due to a geometric path-length asymmetry, elaborated in Sect. 4.

In the real atmosphere, such conditions (low SZA combined with high A_s) occur in low-latitude, high-albedo regions such as salt flats, snow-covered mountains, and deserts near the Tropics of Cancer and Capricorn, particularly around local noon during summer months when the sun approaches zenith.

The magnitude and, in some cases, the sign of the positive ADRF depend on the radiative transfer solver. Figure 1 shows that both DISORT and RODENTS produce qualitatively similar trends: both exhibit positive ADRF at low SZA over high-albedo surfaces. However, there are systematic quantitative differences. At SZA values between approximately 0° and 65°, DISORT yields higher (more positive) ADRF than RODENTS, meaning that the two-stream approximation underestimates the positive forcing in this regime. Conversely, at high SZA (e.g., 85°), DISORT produces more negative ADRF than RODENTS, indicating that the two-stream approximation also underestimates the cooling effect under oblique illumination. This pattern–two-stream methods overestimating cooling at low SZA and underestimating it at high SZA–is consistent with the findings of Randles et al. (2013), who compared 31 radiative transfer schemes and documented analogous systematic biases (e.g., an order of 20% difference at a SZA of 30°, similar to those observed in this study). Since most climate models rely on two-stream-based solvers such as RRTMG for their shortwave radiative transfer calculations (Iacono et al., 2008; Danabasoglu et al., 2020), these biases may propagate into modeled ADRF estimates.

https://doi.org/10.5194/egusphere-2026-3947
Preprint. Discussion started: 14 July 2026

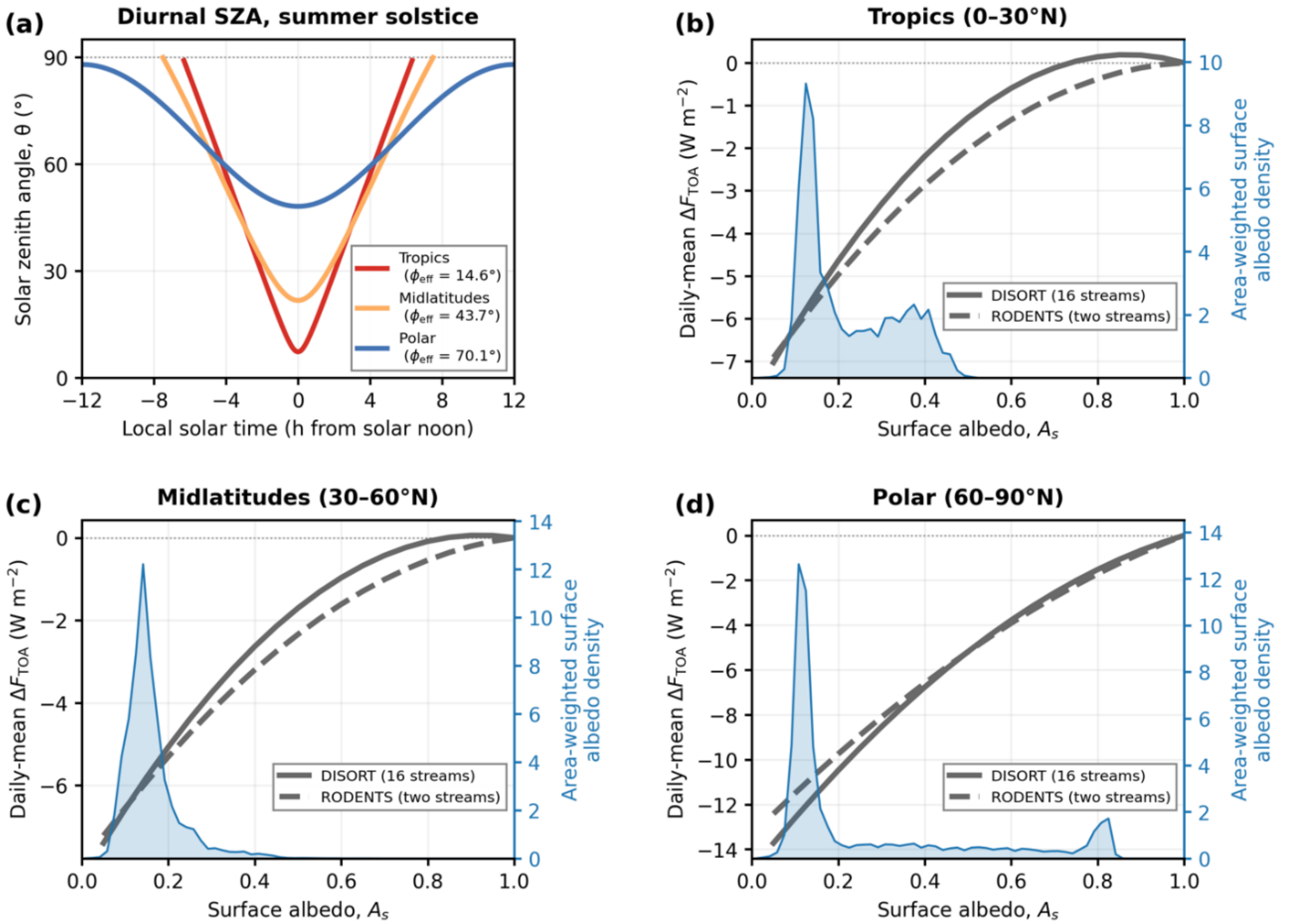

Figure 2. Results of daily-mean latitude averaged ADRF by libRadtran modeling. The method for calculating this averaged ADRF is described in Sect. 2.3. Figure 2a, b and c respectively represent the daily mean ADRF in tropics, middle latitude and polar region in summer solstice day, in northern hemisphere. The solid lines represent DISORT 16 streams solver and dashed lines represent RODENTS two streams solver. The shaded blue area represent the frequency distributions of the surface albedo in the corresponding latitudes.

Studies typically report daily-averaged or longer-term mean radiative forcing to estimate climate impacts. Figure 2 shows the daily-mean ADRF computed for three latitude bands (0–30° N, 30–60° N, 60–90° N) on the northern hemisphere summer solstice. In all three bands, daily averaging substantially attenuates the positive ADRF that is visible at individual SZA values in Fig. 1. This attenuation occurs because the strong negative ADRF at high SZA (morning and evening hours) dominates the time-weighted average, overwhelming the positive forcing that occurs during midday when SZA is low (Fig. 2. Only at very high surface albedo (A_s > ~0.8) does the daily-mean ADRF become positive, and such values are rare outside polar regions. The solver-dependent bias is also attenuated upon daily averaging. In the tropics (Fig. 2b) and midlatitudes (Fig. 2, the daily-mean ADRF from RODENTS remains slightly more negative than DISORT, with the difference being pronounced at high A_s

https://doi.org/10.5194/egusphere-2026-3947
Preprint. Discussion started: 14 July 2026

values. The higher A_s values are uncommon at these latitudes, as shown in the blue shaded frequency distributions on the right y-axes in Fig. 2(b-d). Surface albedo distributions were derived from the MODIS MCD43 BRDF/Albedo product (Schaaf and Wang, 2021), averaged over June–August 2025.In the polar regions (Fig. 2, the DISORT–RODENTS difference is further reduced, and at low albedos (A_s < ~0.2) the sign of the bias reverses; RODENTS yields slightly higher (less negative) ADRF than DISORT. This convergence at high latitudes reflects the dominance of high-SZA conditions in polar diurnal cycles (Fig. 2a), where the two-stream approximation performs comparably to the multi-stream solver.

However, the fact that daily averaging masks these forcing peaks does not render them climatically irrelevant. Because the aerosol layer and atmosphere medium in our simulations is non-absorbing, conservation of energy requires that any reduction in TOA reflected flux corresponds to an equivalent increase in shortwave radiation absorbed at the surface. Positive ADRF at low SZA therefore represents additional surface energy input during peak insolation hours, which is the quantity that governs snowmelt rather than the daily mean (Marks and Dozier, 1992; Bryant et al., 2013). Operational climate models compute shortwave radiative forcing at sub-daily resolution (typically every one to three hours), and snow-hydrology models ingest these fluxes at the same temporal resolution because phase-change processes respond to instantaneous forcing (Tarboton and Luce, 1996; Stigter et al., 2021). Therefore, differences between the instantaneous values obtained by the solvers could lead to errors in calculations of snow and ice dynamics. Only using daily-averaged ADRF in SAI assessments may obscure localized forcing peaks with these implications.

4 Proposed "reflectance asymmetry" mechanism

We demonstrated in Fig. 1 that even a non-absorbing atmosphere causes positive TOA shortwave radiative forcing over high-albedo surfaces at low solar zenith angles. The origin of this effect is a reflectance asymmetry of the aerosol layer: the layer scatters a larger fraction of diffuse upwelling light back toward the surface than it scatters of collimated downwelling light back to space. This asymmetry increases net surface absorption in the surface–atmosphere system, reducing the reflected flux to space relative to the aerosol-free case. We refer to this as the "reflectance asymmetry" mechanism, where the positive forcing arises from the layer's unequal reflectance to downwelling and upwelling radiation, rather than from absorption. Regions where low SZA coincides with high surface albedo – such as low-latitude deserts, salt flats, and snow-covered mountains – are therefore susceptible to this mechanism (Fig. 2b, lower SZA in low-latitude regions).

To quantify the reflectance asymmetry, we propose a physical model using an aerosol slab and a Lambertian reflective surface underneath (illustrated in Fig. 3), also often called a single-layer adding model; we adopt this terminology to maintain consistency with commonly used terms in radiative transfer theory (Buglia, 1982; Zdunkowski et al., 2007).

https://doi.org/10.5194/egusphere-2026-3947
Preprint. Discussion started: 14 July 2026

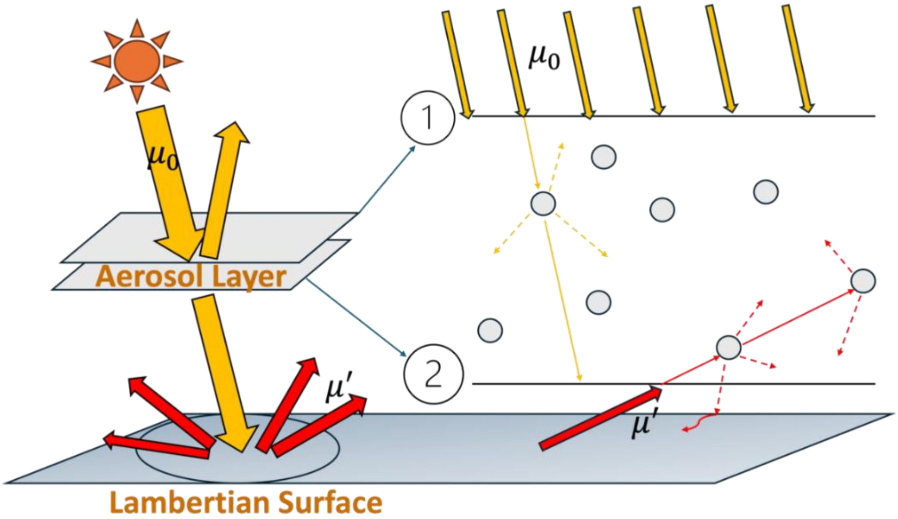

Figure 3. Illustration of the single-layer adding model and the direction-dependent reflectance of the aerosol layer. Scenario 1 (top): collimated solar illumination from above. Orange arrows indicate the solar source and subsequent scattering events within the layer before light reaches the ground surface. Scenario 2 (bottom): diffuse Lambertian illumination from below. Red arrows indicate the secondary source arising from ground surface reflection and subsequent scattering events within the layer. The effective optical path length through the layer is modulated by the incident angle (represented by μ_0 and μ').

4.1 Single-layer adding model

The atmosphere – including aerosol and gases – is represented as a single homogeneous plane-parallel slab above the ground. We define the slab's reflectance as R (the ratio of reflected energy to incident energy) and its transmittance as T. We neglect absorption by the layer for now; however, we discuss its possible implications later in the manuscript.

Let the incident solar irradiance at the TOA be S(μ) and the total upward irradiance at the TOA be $E(A_S,\mu)$. The ratio E/S can be expressed as the sum of the direct reflection R from the layer, and all subsequent transmitted beams of the surface reflected radiation with surface albedo A_S. This can be represented as:

$$\frac{E(A_S,\mu)}{S(\mu)} = R + A_S T^2 + A_S T^2 (R A_S) + A_S T^2 (R A_S)^2 + \cdots\cdots \tag{1}$$

The right hand side is a Geometric Series, which can be written as:

$$A_S T^2 + A_S T^2 (R A_S) + A_S T^2 (R A_S)^2 + \cdots\cdots = As\, T^2 \sum_{n=0}^{\infty} (R A_s)^n = \frac{As\, T^2}{1 - R\, A_s} \tag{2}$$

Therefore, we obtain:

$$E(A_S,\mu) = S(\mu) \left(R + \frac{As\, T^2}{1 - R\, A_s} \right) \tag{3}$$

https://doi.org/10.5194/egusphere-2026-3947
Preprint. Discussion started: 14 July 2026

4.2 Reflectance asymmetry between downwelling and upwelling Radiation

In the single-layer model of Eq. (3), a single reflectance R is used for both downwelling and upwelling light. However, when the solar zenith angle is small, the angular distributions of downwelling and upwelling radiation are fundamentally different, producing different effective reflectances.

The fraction of collimated sunlight arriving from above that is scattered back upward by the aerosol layer is the effective reflectance of the downwelling radiation ($R\downarrow$). At low SZA, this beam traverses the layer along a short, near-vertical path. For an optically thin layer (typical of clear-sky conditions), the scattering probability per photon is small, and $R\downarrow$ is correspondingly low. Meanwhile, the fraction of diffuse upwelling light – sunlight reflected by the Lambertian ground surface – that is scattered back downward by the aerosol layer toward the ground is defined as $R\uparrow$. Because a Lambertian surface reflects radiation isotropically into the upper hemisphere, the upwelling photons travel through the layer at a wide distribution of angles, many of them oblique. An oblique path through a layer of vertical thickness Δz is longer by a factor of $1/\cos(\theta)$, so a significant fraction of the upwelling photons traverses a longer optical path than the collimated beam. This increases their scattering probability, making $R\uparrow > R\downarrow$ when SZA is small.

The key physical point is that at low SZA, the collimated downwelling beam takes a short path (low scattering probability, low $R\downarrow$), while the diffuse upwelling light includes many oblique rays with long paths (high scattering probability, high $R\uparrow$). This asymmetry traps additional radiation between the layer and the surface, enhancing surface absorption. Conversely, as SZA increases, the downwelling beam becomes more oblique and its path through the layer lengthens, so $R\downarrow$ rises. The upwelling diffuse light, by contrast, remains Lambertian and its mean path length through the layer does not depend on SZA. The asymmetry between downwelling and upwelling reflectance therefore weakens as SZA grows, and it is this geometric weakening that causes the positive ADRF identified in Fig. 1 to be confined to small SZA.

4.3 Single-layer adding model with reflectance asymmetry

Upon distinguishing the reflectance and transmittance for downwelling (↓) and upwelling (↑) illumination, equation (3) becomes:

$$E(A_s, \mu) = S(\mu)\,(R_\downarrow + \frac{T_\downarrow T_\uparrow A_s}{1 - R_\uparrow A_s}) \tag{4}$$

where $T_\downarrow, T_\uparrow, R_\downarrow$ and $R_\uparrow$ are the hemispheric transmittance and reflectance for top and bottom illumination, respectively.

Since we assume absorption to be negligible, (as Dykema et al assumed pure scattering alumina particle in visible band), energy closure gives:

$$T_\downarrow = 1 - R_\downarrow, \qquad T_\uparrow = 1 - R_\uparrow \tag{5}$$

Inserting (5) into (4), and applying a partial derivate with respect to $R_\uparrow$ (treating $R_\uparrow$ as an independent variable), we get

https://doi.org/10.5194/egusphere-2026-3947
Preprint. Discussion started: 14 July 2026

$$E(A_s, \mu) = S(\mu)\ [R_\downarrow + \frac{(1-R_\downarrow)(1-R_\uparrow)A_s}{1-R_\uparrow A_s}] \tag{6}$$

$$\frac{\partial E}{\partial R_\uparrow} = S(\mu)\ [(1-R_\downarrow)A_s \frac{A_s-1}{(1-R_\uparrow A_s)^2}] \tag{7}$$

For $0 \leq A_s \leq 1$, one can find $\frac{\partial E}{\partial R_\uparrow} \leq 0$.

We define the reflectance asymmetry parameter Φ as the ratio between $R_\uparrow$ and $R_\downarrow$:

$$\Phi \equiv \frac{R_\uparrow}{R_\downarrow} \tag{8}$$

Then

$$\frac{\partial E}{\partial R_\uparrow} = S(\mu)\ [(1-R_\downarrow)A_s \frac{A_s-1}{(1-R_\uparrow A_s)^2}] < 0 \Rightarrow \frac{\partial E}{\partial \Phi} = R_\downarrow \frac{\partial E}{\partial R_\uparrow} < 0 \tag{9}$$

Thus, increasing Φ lowers E (and lowers radiative forcing) for any $A_s < 1$. Physically, the more asymmetric the layer's reflectance (larger Φ), the more radiation is trapped between the surface and the layer, reducing the flux escaping to space. In the absorption-free limit, any reduction in TOA flux maps directly onto increased surface absorption, so the path-length asymmetry quantified by Φ provides a physical mechanism for the enhanced surface energy deposition discussed in Sect. 3.

From Eq. (4), $R\downarrow$ can be obtained directly:

$$R_\downarrow = E(A_s = 0, \mu)\ /\ S(\mu) \tag{10}$$

Hence, we can use a radiative transfer model with zero ground surface albedo to calculate the value of $R_\downarrow$.

Using Eq. (6) and the value of $R_\downarrow$, we can have $R_\uparrow$ expression as:

$$R_\uparrow = \frac{R_\downarrow + (1-R_\downarrow)A_s - E(A_s,\mu)/S(\mu)}{A_s[1-\frac{E(A_s,\mu)}{S(\mu)}]} \tag{11}$$

4.4 Model validation

Using the numerical radiative transfer simulations described in Sect. 2, we compute $E(A_s, \mu)$ for each combination of A_s and SZA. From these, $R\downarrow$ is obtained via Eq. (10) and $R\uparrow$ via Eq. (11), yielding Φ from Eq. (8). The extracted reflectances are shown separately in Fig. S3: $R\downarrow$ increases monotonically with SZA, reflecting the lengthening slant path of the collimated beam, whereas $R\uparrow$ is constant across both SZA and surface albedo.

The model makes a testable prediction: because Φ characterizes only the angular scattering properties of the aerosol layer itself, it should depend on SZA and on the radiative transfer solver used, but be independent of the underlying surface albedo. Figure 4 confirms this prediction. Panel (a) shows Φ as a function of SZA for both DISORT and RODENTS. At low SZA, Φ is substantially greater than unity ($\Phi \approx 2.0$ for DISORT at SZA = 5°), confirming that the layer reflects a much larger fraction of diffuse upwelling light than collimated downwelling light. As SZA increases, Φ decreases monotonically, crossing unity near SZA ≈ 55–60° for DISORT (≈ 45° for RODENTS), where the beam's slant path matches the effective path of the diffuse field, and falling below unity at larger SZA, where $R\downarrow$ exceeds $R\uparrow$ (Fig. S3) and the layer reflects the direct beam more strongly than the diffuse upwelling field — consistent with the negative ADRF at high SZA (Fig.1 and Fig. S2). The DISORT multi-

https://doi.org/10.5194/egusphere-2026-3947
Preprint. Discussion started: 14 July 2026

stream solver captures the angular dependence of the reflectance asymmetry more accurately than a two-stream approximation. Figure 4(b) shows Φ as a function of A_s for three representative SZA values. For each SZA, Φ remains constant across all surface albedo values, confirming the model prediction that the reflectance asymmetry is an intrinsic property of the aerosol layer and is independent of the surface below it.

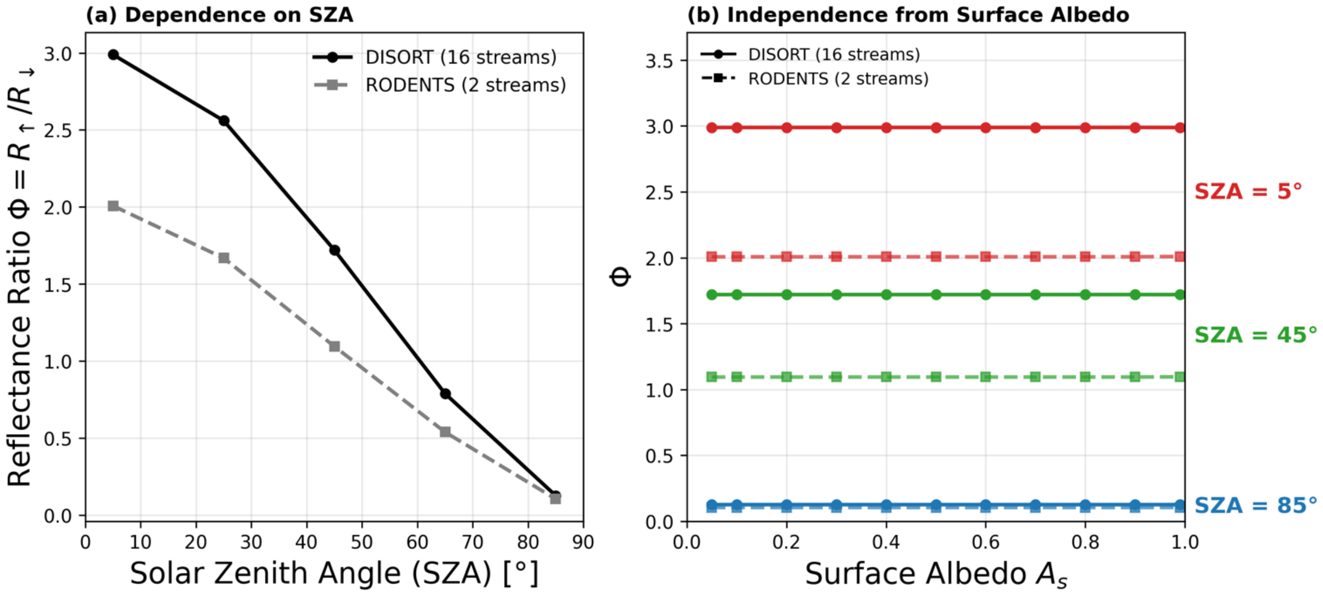

Figure 4. Dependence of the reflectance ratio parameter Φ on solar zenith angle and surface albedo. (a) Φ as a function of SZA, illustrating the systematic bias between DISORT (solid) and RODENTS (dashed) solvers. (b) Φ as a function of surface albedo (A_s) for three representative SZA values (5°,45°,85°). Note that Φ remains constant with respect to As , confirming the model prediction that reflectance asymmetry is independent of the underlying surface albedo.

5 Conclusions

This study demonstrates that stratospheric aerosol injection using purely scattering particles can produce positive shortwave radiative forcing over high-albedo surfaces at low solar zenith angles. Positive forcing over high-albedo regions following stratospheric aerosol injection has previously been reported in global simulations (Brovkin et al., 2009) and in satellite analyses of the aerosol direct radiative effect (Chen et al., 2024), with both attributing the positive forcing to surface-amplified absorption by weakly absorbing aerosols. The counter-intuitive result demonstrated here – a net reduction in reflected flux to space despite zero aerosol absorption – has not previously been explained from first principles. Current assessments of SAI primarily focus on risks such as ozone depletion, precipitation pattern changes, and cloud formation impacts (Robock et al., 2008); the potential localized positive forcing due to the reflectance asymmetry mechanism identified here represents an additional risk not captured in current assessments.

https://doi.org/10.5194/egusphere-2026-3947
Preprint. Discussion started: 14 July 2026

To elucidate the mechanism leading to a potential warming by SAI particles, we derived a single-layer adding model that attributes the positive forcing to an optical path length asymmetry between collimated downwelling solar radiation and diffuse upwelling radiation. We defined a reflectance ratio parameter $\Phi = R\uparrow/R\downarrow$ that quantifies this asymmetry and showed analytically that increasing Φ reduces the TOA reflected flux for any sub-unity surface albedo (Eq. 9). The model predicts that Φ should be independent of surface albedo – a prediction confirmed by numerical radiative transfer simulations (Fig. 4b). Further validation of the mechanism would help to improve our understanding of the mechanism in the real-world, and its radiative impact. Direct observational verification of this mechanism may have methodological challenges related to disentangling atmospheric absorption from reflectance asymmetry – for example by stratifying satellite-derived forcing by retrieved single-scattering albedo. We leave this verification to future work.

Our simulations also reveal that the two-stream approximation (RODENTS) systematically underestimates the positive forcing relative to the 16-stream DISORT solver. Since most climate models rely on two-stream radiative transfer schemes, this bias may propagate into modeled estimates of SAI radiative forcing. Furthermore, conventional daily-averaged forcing metrics attenuate the diurnal peaks of positive ADRF, potentially obscuring impacts on processes governed by instantaneous energy fluxes, such as snowmelt (Marks and Dozier, 1992; Bryant et al., 2013; Tarboton and Luce, 1996; Stigter et al., 2021). The relevance of these results extends beyond deliberate injection. Any optically thin, highly scattering particle layer above a high-albedo surface is subject to the same reflectance asymmetry. For example, alumina from spacecraft reentry, already detected in stratospheric aerosol (Murphy et al., 2023) and increasing with launch activity, is a natural candidate. Present-day reentry-derived loadings (Maloney et al., 2025) remain orders of magnitude below those considered for SAI (Dykema et al., 2016; Vattioni et al., 2024), and the corresponding forcing scales with layer optical depth; the sign structure identified here – positive rather than negative shortwave forcing over bright surfaces – nevertheless applies to these sources as they grow.

Recent measurements indicate that alumina exhibits weak but nonzero shortwave absorption, with an imaginary refractive index on the order of 10^{-4} (Kapoor et al., 2026). Although this absorption is small, our libRadtran simulations show that multiple scattering amplifies its effect over bright surfaces (Fig. S1). Combined with the scattering-induced ground absorption mechanism described here, even weak particle absorption, due to defects (Kapoor et al., 2026) or impurities (Kumar et al., 2026) can further enhance positive TOA radiative forcing.

Several limitations of this study should be noted. The radiative transfer model is offline and instantaneous: it does not account for particle transport, atmospheric dynamics, heat conduction, or latent heat processes that would be resolved in GCMs. No background atmospheric molecular scattering or absorption is included, so the absolute magnitudes of ADRF reported here should be interpreted as indicative of trends rather than quantitative predictions. We note, however, that the underlying surface assumed here may be understood as a representative absorbing atmosphere plus reflective surface layer.. Additionally, this study does not include clouds. Clouds possess high albedo (0.4–0.9 depending on thickness, water content, and type) (Hartmann et al., 2016) and reside at altitudes (2–12 km) below the modeled SAI injection height. The mechanism described here implies that the aerosol layer would also enhance absorption at cloud tops. Since the same path-length asymmetry applies, collimated sunlight passes through the aerosol layer on a short path, while diffuse light reflected upward by the cloud top

https://doi.org/10.5194/egusphere-2026-3947
Preprint. Discussion started: 14 July 2026

traverses longer, more oblique paths. Low-latitude clouds would experience the most significant effect, as they are illuminated at the lowest SZA values where the reflectance asymmetry Φ is largest (Fig. 4a). However, cloud surfaces are better described as bidirectional reflectors than Lambertian surfaces (Suttles et al., 1988), so the quantitative application of this mechanism to clouds would require explicit treatment of the cloud bidirectional reflectance distribution function.

Code availability

The libRadtran radiative transfer package (Emde et al., 2016) is freely available at http://www.libradtran.org. The PyMisScatt python package (Sumlin et a., 2018) is available for download at https://github.com/bsumlin/PyMieScatt.

Data availability

The MODIS MCD43C3 surface albedo product (Schaaf and Wang, 2021) is available from the NASA Land Processes Distributed Active Archive Center at https://doi.org/10.5067/MODIS/MCD43C3.061.

Author contribution

LZ: Methodology, Software, Formal Analysis, Writing - Original Draft; TSK: Validation, Writing - Review & Editing, Supervision; PU: Validation, Writing - Review & Editing; RKC: Conceptualization, Writing - Review & Editing, Supervision, Funding acquisition.

Competing interests

The authors declare that they have no conflict of interest.

Acknowledgements

The authors thank Joshin Kumar for assistance with radiative transfer modeling.

Financial support

This research has been supported by the Simons Foundation (grant number. SFI-MPS-SRM-00005174).

https://doi.org/10.5194/egusphere-2026-3947
Preprint. Discussion started: 14 July 2026

References

Atwater, M. A.: Planetary albedo changes due to aerosols, Science, 170, 64–66, https://doi.org/10.1126/science.170.3953.64, 1970.

Brovkin, V., Petoukhov, V., Claussen, M., Bauer, E., Archer, D., and Jaeger, C.: Geoengineering climate by stratospheric sulfur injections: Earth system vulnerability to technological failure, Clim. Change, 92, 243–259, https://doi.org/10.1007/s10584-008-9490-1, 2009.

Bryant, A. C., Painter, T. H., Deems, J. S., and Bender, S. M.: Impact of dust radiative forcing in snow on accuracy of operational runoff prediction in the Upper Colorado River Basin, Geophys. Res. Lett., 40, 3945–3949, https://doi.org/10.1002/grl.50773, 2013.

Buglia, J. J.: A tutorial solution to scattering of radiation in a thin atmosphere bounded below by a diffusely reflecting, absorbing surface, NASA Technical Paper 2077, National Aeronautics and Space Administration, 1982.

Chen, A., Zhao, C., Zhang, H., Yang, Y., and Li, J.: Surface albedo regulates aerosol direct climate effect, Nat. Commun., 15, 7816, https://doi.org/10.1038/s41467-024-52255-z, 2024.

Crutzen, P. J.: Albedo enhancement by stratospheric sulfur injections: a contribution to resolve a policy dilemma?, Clim. Change, 77, 211–220, https://doi.org/10.1007/s10584-006-9101-y, 2006.

Danabasoglu, G., Lamarque, J.-F., Bacmeister, J., Bailey, D. A., DuVivier, A. K., Edwards, J., Emmons, L. K., et al.: The Community Earth System Model Version 2 (CESM2), J. Adv. Model. Earth Sy., 12, e2019MS001916, https://doi.org/10.1029/2019MS001916, 2020.

Derimian, Y., Dubovik, O., Huang, X., Lapyonok, T., Litvinov, P., Kostinski, A. B., Dubuisson, P., and Ducos, F.: Comprehensive tool for calculation of radiative fluxes: illustration of shortwave aerosol radiative effect sensitivities to the details in aerosol and underlying surface characteristics, Atmos. Chem. Phys., 16, 5763–5780, https://doi.org/10.5194/acp-16-5763-2016, 2016.

Duffie, J. A. and Beckman, W. A.: Solar Engineering of Thermal Processes, 4th edn., John Wiley & Sons, Hoboken, New Jersey, USA, 2013.

Dykema, J. A., Keith, D. W., and Keutsch, F. N.: Improved aerosol radiative properties as a foundation for solar geoengineering risk assessment, Geophys. Res. Lett., 43, 7758–7766, https://doi.org/10.1002/2016GL069258, 2016.

Emde, C., Buras-Schnell, R., Kylling, A., Mayer, B., Gasteiger, J., Hamann, U., Kylling, J., Richter, B., Pause, C., Dowling, T., and Bugliaro, L.: The libRadtran software package for radiative transfer calculations (version 2.0.1), Geosci. Model Dev., 9, 1647–1672, https://doi.org/10.5194/gmd-9-1647-2016, 2016.

Hartmann, D. L.: Global Physical Climatology, 2nd edn., Elsevier, Amsterdam, the Netherlands, https://doi.org/10.1016/C2009-0-00030-0, 2016.

https://doi.org/10.5194/egusphere-2026-3947
Preprint. Discussion started: 14 July 2026

Iacono, M. J., Delamere, J. S., Mlawer, E. J., Shephard, M. W., Clough, S. A., and Collins, W. D.: Radiative forcing by long-lived greenhouse gases: calculations with the AER radiative transfer models, J. Geophys. Res.-Atmos., 113, D13103, https://doi.org/10.1029/2008JD009944, 2008.

Kapoor, T. S., Upadhyay, P., Huang, J., Ren, G., Cavin, J., Mitroo, D., Vattioni, S., Dykema, J., Sedlacek, J., Kumar, J., Hachtel, J. A., Xu, L., Mishra, R., and Chakrabarty, R. K.: Unveiling the shortwave absorption spectra of alumina aerosols: implications for solar radiation modification, arXiv [preprint], https://doi.org/10.48550/arXiv.2509.24246, 2026.

Kumar, J., Jung, G. Y., Kapoor, T. S., Mishra, R., and Chakrabarty, R. K.: Strong light absorption by sp2 hybridized carbon impurities in diamond dust, J. Aerosol Sci., 106767, https://doi.org/10.1016/j.jaerosci.2026.106767, 2026.

Marks, D. and Dozier, J.: Climate and energy exchange at the snow surface in the alpine region of the Sierra Nevada: 2. Snow cover energy balance, Water Resour. Res., 28, 3043–3054, https://doi.org/10.1029/92WR01483, 1992.

Murphy, D. M., Abou-Ghanem, M., Cziczo, D. J., Froyd, K. D., Jacquot, J., Lawler, M. J., Maloney, C., Plane, J. M. C., Ross, M. N., Schill, G. P., and Shen, X.: Metals from spacecraft reentry in stratospheric aerosol particles, P. Natl. Acad. Sci. USA, 120, e2313374120, https://doi.org/10.1073/pnas.2313374120, 2023.

Oke, T. R.: Guide to instruments and methods of observation, Volume III, WMO-No. 8, World Meteorological Organization, Geneva, Switzerland, 2018.

Pope, F. D., Braesicke, P., Grainger, R. G., Kalberer, M., Watson, I. M., Davidson, P. J., and Cox, R. A.: Stratospheric aerosol particles and solar-radiation management, Nat. Clim. Change, 2, 713–719, https://doi.org/10.1038/nclimate1528, 2012.

Randles, C. A., Kinne, S., Myhre, G., Schulz, M., Stier, P., Fischer, J., Doppler, L., Highwood, E., Ryder, C., Harris, B., Huttunen, J., Ma, Y., Pinker, R. T., Mayer, B., Neubauer, D., Hitzenberger, R., Oreopoulos, L., Lee, D., Pitari, G., Di Genova, G., Quaas, J., Rose, F. G., Kato, S., Rumbold, S. T., Vardavas, I., Hatzianastassiou, N., Matsoukas, C., Yu, H., Zhang, F., Zhang, H., and Lu, P.: Intercomparison of shortwave radiative transfer schemes in global aerosol modeling: results from the AeroCom Radiative Transfer Experiment, Atmos. Chem. Phys., 13, 2347–2379, https://doi.org/10.5194/acp-13-2347-2013, 2013.

Robock, A.: Volcanic eruptions and climate, Rev. Geophys., 38, 191–219, https://doi.org/10.1029/1998RG000054, 2000.

Schaaf, C. and Wang, Z.: MODIS/Terra+Aqua BRDF/Albedo Albedo Daily L3 Global 0.05Deg CMG V061, NASA Land Processes Distributed Active Archive Center [data set], https://doi.org/10.5067/MODIS/MCD43C3.061, 2021.

Stamnes, K., Tsay, S.-C., Wiscombe, W., and Jayaweera, K.: Numerically stable algorithm for discrete-ordinate-method radiative transfer in multiple scattering and emitting layered media, Appl. Optics, 27, 2502–2509, https://doi.org/10.1364/AO.27.002502, 1988.

Stigter, E. E., Steiner, J. F., Koch, I., Saloranta, T. M., Kirkham, J. D., and Immerzeel, W. W.: Energy and mass balance dynamics of the seasonal snowpack at two high-altitude sites in the Himalaya, Cold Reg. Sci. Technol., 183, 103233, https://doi.org/10.1016/j.coldregions.2021.103233, 2021.

https://doi.org/10.5194/egusphere-2026-3947
Preprint. Discussion started: 14 July 2026

Sumlin, B. J., Heinson, W. R., and Chakrabarty, R. K.: Retrieving the aerosol complex refractive index using PyMieScatt: a Mie computational package with visualization capabilities, J. Quant. Spectrosc. Ra., 205, 127–134, https://doi.org/10.1016/j.jqsrt.2017.10.012, 2018.

Suttles, J. T., Green, R. N., Minnis, P., Smith, G. L., Staylor, W. F., Wielicki, B. A., Walker, I. J., Young, D. F., Taylor, V. R., and Stowe, L. L.: Angular radiation models for Earth-atmosphere system, Volume I: shortwave radiation, NASA Reference Publication 1184, https://ntrs.nasa.gov/citations/19880018292 (last access: 11 June 2026), 1988.

Tarboton, D. G. and Luce, C. H.: Utah Energy Balance Snow Accumulation and Melt Model (UEB): computer model technical description and users guide, Utah Water Research Laboratory and USDA Forest Service Intermountain Research Station, 1996.

Tropf, W. J. and Thomas, M. E.: Aluminum oxide (Al2O3) revisited, in: Handbook of Optical Constants of Solids, edited by: Palik, E. D., Academic Press, 653–682, https://doi.org/10.1016/B978-012544415-6.50124-2, 1997.

Vattioni, S., Weber, R., Feinberg, A., Stenke, A., Dykema, J. A., Luo, B., Kelesidis, G. A., Bruun, C. A., Sukhodolov, T., Keutsch, F. N., Peter, T., and Chiodo, G.: A fully coupled solid-particle microphysics scheme for stratospheric aerosol injections within the aerosol–chemistry–climate model SOCOL-AERv2, Geosci. Model Dev., 17, 7767–7793, https://doi.org/10.5194/gmd-17-7767-2024, 2024.

Weisenstein, D. K., Keith, D. W., and Dykema, J. A.: Solar geoengineering using solid aerosol in the stratosphere, Atmos. Chem. Phys., 15, 11835–11859, https://doi.org/10.5194/acp-15-11835-2015, 2015.

Zdunkowski, W., Trautmann, T., and Bott, A.: Radiation in the Atmosphere: A Course in Theoretical Meteorology, Cambridge University Press, Cambridge, UK, 2007.